

The *Echo 12–23 Texture*: A Novel Flavour Paradigm for Neutrinos

Manash Dey* and Subhankar Roy†
Department of Physics, Gauhati University, India.
(Dated: July 2, 2025)

We construct a flavour guided model that realises the distinctive *Echo 12–23 Texture* in the neutrino mass matrix through a non-trivial interplay of symmetries. While the model accounts for charged lepton mass hierarchy, the texture offers interesting insights specifically into neutrino mass ordering and flavour dynamics. With clear imprints on low energy observables, the framework provides a minimal yet testable path toward understanding the origin of neutrino properties.

I. INTRODUCTION

The Standard Model (SM) [1–5] of particle physics, based on the gauge group $SU(3)_C \times SU(2)_L \times U(1)_Y$, has successfully described a wide range of phenomena involving fundamental particles and interactions. However, several observations remain unexplained within its framework, including the origin of neutrino [6] masses, the nature of their mass ordering, and the hierarchy among charged lepton masses. Notably, neutrino oscillation experiments have firmly established that neutrinos are massive and undergo flavour transitions [7–9], necessitating an extension beyond the SM. Among various beyond SM (BSM) approaches, seesaw mechanisms [10, 11] provide elegant explanations for the smallness of neutrino masses. In particular, the Type-I seesaw [12, 13] introduces heavy right handed neutrinos (ν_R), while the Type-II seesaw [13, 14] relies on an $SU(2)_L$ scalar triplet (Δ) acquiring a small vacuum expectation value (vev). The typical Feynman diagrams for the Type-I and Type-II seesaw are shown in Fig. 1. An interesting scenario combining both, commonly known as the Type-I+II seesaw mechanism [15–18], offers increased structural richness and emerges naturally in symmetry driven frameworks. The neutrino mass matrix, M_ν , encodes valuable information about mixing angles ($\theta_{12}, \theta_{13}, \theta_{23}$), CP violating phases (δ, α, β), and the neutrino mass eigenvalues (m_1, m_2, m_3). However, neutrino oscillation data constrains only a subset of these parameters. To bridge this gap, various theoretical strategies have been explored, most notably the introduction of textures, where specific correlations or patterns in the matrix elements reduce parameter freedom and enhances the predictive power [19–23].

In this work, we propose a flavour motivated model embedded within a Type-I+II seesaw framework, where a discrete symmetry structure gives rise to a distinctive neutrino mass texture. This texture imposes strong constraints on the neutrino mixing parameters. Moreover, the model naturally reproduces the observed charged lepton mass hierarchy through symmetry protected suppressions. We also explore the phenomenological consequences of the texture, particularly its imprints on low energy observables such as neutrinoless double beta ($0\nu\beta\beta$) decay and charged lepton flavour violation (cLFV).

The structure of the paper is as follows: in Section II, we introduce the model and the underlying symmetry groups, and discuss the construction of the model in detail. Section III contains the numerical analysis and the predictions of the model. In Sections IV and V, we discuss the implications for $0\nu\beta\beta$ decay and cLFV respectively. Finally, in Section VI, we present a summary and discussion of our findings.

II. THEORETICAL FRAMEWORK

We extend the Standard Model (SM) gauge group by incorporating an A_4 flavour symmetry [24–27] along with cyclic Z_N [28–33] symmetries, particularly Z_3 [30–32] and Z_{10} [30–32]. The complete symmetry group of the model is given by

$$\mathcal{G} = A_4 \times Z_3 \times Z_{10} \times SU(2)_L \times U(1)_Y. \quad (1)$$

The SM field content is augmented by introducing $SU(2)_L$ singlet right handed neutrino fields (ν_{lR}) and five $SU(2)_L$ singlet scalar fields ($\chi, \kappa, \sigma, \rho, \zeta$). In addition, we introduce an extra $SU(2)_L$ doublet Φ and a triplet Δ . The cyclic symmetries play a crucial role in restricting potential next to leading order (NLO) corrections, which could otherwise perturb the Yukawa Lagrangian (\mathcal{L}_Y). The transformation properties of the field content under the full symmetry of

* manashdey@gauhati.ac.in

† subhankar@gauhati.ac.in

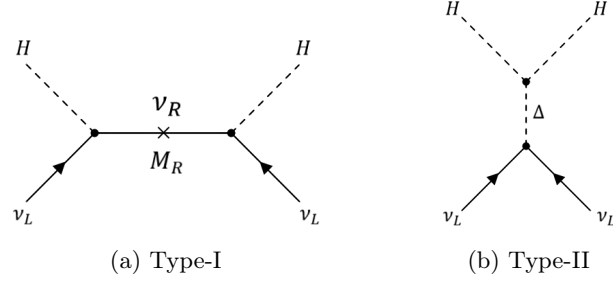


FIG. 1. Feynman diagrams for Type-I and Type-II seesaw mechanisms.

| Field | D_{l_L} | l_R | H | ν_{l_R} | Φ | Δ | χ | κ | σ | ρ | ζ |
|-----------|-----------|----------------|-----|---------------------------|------------|------------|------------|------------|----------|----------|------------|
| A_4 | 3 | $(1, 1'', 1')$ | 3 | $(1, 1'', 1')$ | 3 | 3 | $1'$ | $1''$ | 1 | 1 | 1 |
| Z_3 | ω | ω | 1 | $(1, \omega^*, \omega^*)$ | ω^* | ω^* | ω^* | ω^* | ω | ω | ω^* |
| Z_{10} | 0 | $(1, 4, 7)$ | 0 | $(0, 2, 7)$ | 0 | 0 | 6 | 6 | 8 | 3 | 1 |
| $SU(2)_L$ | 2 | 1 | 2 | 1 | 2 | 3 | 1 | 1 | 1 | 1 | 1 |
| $U(1)_Y$ | -1 | -2 | 1 | 0 | -1 | -2 | 0 | 0 | 0 | 0 | 0 |

TABLE I. Transformation properties of the fields under \mathcal{G} .

the model are summarized in Table I. The leading order (LO) \mathcal{L}_Y is constructed in the Altarelli–Feruglio basis of A_4 , and is presented as shown below

$$-\mathcal{L}_Y = \mathcal{L}_l + \mathcal{L}_\nu + h.c. \quad (2)$$

Here, \mathcal{L}_l and \mathcal{L}_ν correspond to the charged lepton and neutrino sectors, respectively, and are structured as follows,

$$\mathcal{L}_l = y_e \bar{D}_{l_L} H e_R \left(\frac{\zeta}{\Lambda}\right)^9 + y_\mu \bar{D}_{l_L} H \mu_R \left(\frac{\zeta}{\Lambda}\right)^6 + y_\tau \bar{D}_{l_L} H \tau_R \left(\frac{\zeta}{\Lambda}\right)^3, \quad (3)$$

and

$$\begin{aligned} \mathcal{L}_\nu = & y_{D_1} \bar{D}_{l_L} \Phi \nu_{eR} + y_{D_2} \bar{D}_{l_L} \Phi \nu_{\mu R} \left(\frac{\sigma}{\Lambda}\right) + y_{D_3} \bar{D}_{l_L} \Phi \nu_{\tau R} \left(\frac{\rho}{\Lambda}\right) + \frac{1}{2} \overline{\nu_{eR}^C} \nu_{eR} + \frac{1}{2} y_1 \overline{\nu_{\mu R}^C} \nu_{\tau R} \zeta + \frac{1}{2} y_1 \overline{\nu_{\tau R}^C} \nu_{\mu R} \zeta + \\ & \frac{1}{2} y_2 \overline{\nu_{\mu R}^C} \nu_{\mu R} \kappa + \frac{1}{2} y_3 \overline{\nu_{\tau R}^C} \nu_{\tau R} \chi + y_\Delta \bar{D}_{l_L} D_{l_L}^C i \sigma_2 \Delta, \end{aligned} \quad (4)$$

where Λ is the effective scale of the theory. The symmetry of \mathcal{L}_Y is spontaneously broken when the scalar fields acquire their respective vevs. A possible complete symmetry breaking pattern of the present model is shown below

$$\begin{aligned} & \mathcal{G} \\ & \downarrow \langle \zeta \rangle \\ & SU(2)_L \times U(1)_Y \times A_4 \\ & \downarrow \langle \sigma, \rho, \chi, \kappa \rangle \\ & SU(2)_L \times U(1)_Y \\ & \downarrow \langle \Phi, \Delta \rangle \langle H \rangle \\ & U(1)_{\text{em}} \end{aligned} \quad (5)$$

It is to be noted that the Z_3 and Z_{10} symmetries of \mathcal{L}_Y are broken by the vev of the scalar singlet ζ . This breaking is important for the explanation of the charged lepton mass hierarchy [34, 35]. For the following vacuum alignments: $\langle H \rangle = v_h(1, 0, 0)^T$, $\langle \Phi \rangle = v_\Phi(0, 0, 1)^T$, $\langle \Delta \rangle = v_\Delta(-1, 0, -1)^T$, $\langle \chi \rangle = v_\chi$, $\langle \kappa \rangle = v_\kappa$, $\langle \sigma \rangle = v_\sigma$, $\langle \rho \rangle = v_\rho$, $\langle \zeta \rangle = v_\zeta$, one

can derive the structure of the fermion mass matrices. The model predicts a diagonal charged lepton mass matrix, with masses satisfying the hierarchical relation

$$m_e : m_\mu : m_\tau = \lambda_f^6 y_e : \lambda_f^3 y_\mu : y_\tau, \quad (6)$$

where $\lambda_f = v_\zeta/\Lambda$. This relation can successfully account for the observed hierarchy [36, 37] among the charged lepton masses.

The complex symmetric Majorana neutrino mass matrix in the Type-I+II seesaw framework is given by $M_\nu = M_{II} - M_D M_R^{-1} M_D^T$, where M_D , M_R , and M_{II} denote the Dirac neutrino mass matrix, the right handed Majorana neutrino mass matrix, and the mass matrix arising from the Type-II seesaw mechanism, respectively. In the present model, the effective Type-I+II neutrino mass matrix takes the following form

$$M_\nu = \begin{pmatrix} r - 2t & t & -q \\ t & -p & t \\ -q & t & s - 2t \end{pmatrix}, \quad (7)$$

where

$$p = \frac{y_{D_1}^2 v_\Phi^2}{M_1}, \quad (8)$$

$$q = \frac{y_{D_2} y_{D_3} y_1 v_\Phi^2 v_\rho v_\sigma v_\zeta}{((y_1 v_\zeta)^2 - y_2 y_3 v_\kappa v_\chi) \Lambda^2}, \quad (9)$$

$$r = \frac{y_{D_3}^2 y_2 v_\Phi^2 v_\rho^2 v_\kappa}{((y_1 v_\zeta)^2 - y_2 y_3 v_\kappa v_\chi) \Lambda^2}, \quad (10)$$

$$s = \frac{y_{D_2}^2 y_3 v_\Phi^2 v_\sigma^2 v_\chi}{((y_1 v_\zeta)^2 - y_2 y_3 v_\kappa v_\chi) \Lambda^2}, \quad (11)$$

$$t = y_\Delta v_\Delta. \quad (12)$$

For the sake of simplicity, we refer to the parameters on the right hand side of Eqs. (8)–(12) as model parameters, and those on the left hand side as texture parameters.

The texture in Eq. (7) features a unique relation

$$(M_\nu)_{e\mu} = (M_\nu)_{\mu\tau}. \quad (13)$$

We refer to this type of texture as the *Echo 12–23 Texture* because the (12) and (23) elements of M_ν echo each other through their equality. This correlation may significantly restrict the allowed values of the observable parameters. Before delving into the predictive implications of this texture, we first briefly review the parametrization of the PMNS matrix [38]. According to the Particle Data Group (PDG) [36], the Pontecorvo Maki Nakagawa Sakata (PMNS) matrix (U) is parametrized in the following way

$$U = P_\phi \tilde{U} P_M, \quad (14)$$

where $P_\phi = \text{diag}(e^{i\phi_1}, e^{i\phi_2}, e^{i\phi_3})$ contains the unphysical phases, and $P_M = \text{diag}(e^{i\alpha}, e^{i\beta}, 1)$ encodes the Majorana phases. The arbitrary phases ϕ_i ($i = 1, 2, 3$) are absorbed by redefining the charged lepton fields, simplifying the PMNS matrix to

$$U = \tilde{U} P_M. \quad (15)$$

In the charged lepton diagonal basis, U diagonalizes M_ν as

$$U^T M_\nu U = \text{diag}(m_1, m_2, m_3). \quad (16)$$

This leads to the equivalent condition

$$\tilde{U}^T M_\nu \tilde{U} = \text{diag}(\tilde{m}_1, \tilde{m}_2, m_3), \quad (17)$$

where the rephased masses are defined as $\tilde{m}_1 = m_1 e^{-2i\alpha}$ and $\tilde{m}_2 = m_2 e^{-2i\beta}$. Thus, \tilde{U} is the matrix that diagonalizes the M_ν of our model. The general form of \tilde{U} is shown below

$$\tilde{U} = \begin{bmatrix} c_{12}c_{13} & s_{12}c_{13} & s_{13}e^{-i\delta} \\ -s_{12}c_{23} - c_{12}s_{13}s_{23}e^{i\delta} & c_{12}c_{23} - s_{12}s_{13}s_{23}e^{i\delta} & c_{13}s_{23} \\ s_{12}s_{23} - c_{12}s_{13}c_{23}e^{i\delta} & -c_{12}s_{23} - s_{12}s_{13}c_{23}e^{i\delta} & c_{13}c_{23} \end{bmatrix}, \quad (18)$$

where $c_{ij} = \cos \theta_{ij}$ and $s_{ij} = \sin \theta_{ij}$. The θ_{ij} represents the three mixing angles.

The diagonalizing matrix \tilde{U} imposes constraints on the neutrino mass matrix M_ν , such that all complex texture parameters p, q, r, s , and t can be expressed in terms of only three real parameters: $Re[s], Im[s]$ and $Re[t]$. In other words, these three free parameters are sufficient to fully determine M_ν and its associated predictions.

III. NUMERICAL ANALYSIS

We first perform a numerical analysis in the light of normal hierarchy (NH) of neutrino masses. In this regard, the 3σ ranges of the mixing angles and the Dirac CP phase δ are used as inputs. A large sample of points in the parameter space $Re[s], Im[s], Re[t]$ is generated, requiring that the mass-squared differences Δm_{21}^2 and Δm_{31}^2 lie within the 3σ ranges reported by NuFIT 6.0 [39]. In addition, the sum of the three light neutrino masses is required to satisfy the cosmological bound $\sum m_i < 0.12$ eV [40]. From the dataset, we find that viable parameter points exist within the following ranges

$$\begin{aligned} (Re[s])_{\min} &= 0.0752 \text{ eV}, & (Re[s])_{\max} &= 0.0843 \text{ eV}; \\ (Im[s])_{\min} &= -0.0089 \text{ eV}, & (Im[s])_{\max} &= 0.0086 \text{ eV}; \\ (Re[t])_{\min} &= 0.0192 \text{ eV}, & (Re[t])_{\max} &= 0.0236 \text{ eV}, \end{aligned}$$

However, when performing a similar scan assuming an inverted hierarchy (IH), we find that the model yields no viable parameter points. *Thus, IH is disfavoured in this model.*

It is important to note that, although the mixing angles and δ are scanned over their full 3σ ranges, we observe that for the viable parameter space yielding $\sum m_i$ within the range 0.1 eV to 0.118 eV, the Dirac CP phase δ is strongly restricted. A large portion of its allowed range, approximately between 104° and 285.6° , is forbidden by the model. While δ is typically treated as a free parameter in many flavour models, here its viable values are tightly limited due to the structure of the *Echo 12–23 Texture*. As a result, the overall parameter space through this restriction on δ is also constrained. From the predicted spectra of the neutrino mass eigenvalues, m_1 and m_2 appears to overlap in certain regions, potentially giving the impression of an exact degeneracy. However, when we calculate $m_2 - m_1$, the difference is never zero, thereby removing the notion of exact degeneracy. This supports a quasi-degenerate mass spectra, i.e., $m_1 \lesssim m_2 \lesssim m_3$. The model predicts the Majorana phases within a narrow range. The phases α and β are constrained to lie between -90° and 90° and -12.7° and 13.6° , respectively. Since the Dirac CP phase δ is subject to restrictions, we also study the associated Jarlskog invariant J_{CP} , which quantifies leptonic CP violation and depends directly on δ and the mixing angles. The J_{CP} is predicted to lie between -0.0324 and 0.030 . To summarize our findings, we list the numerical values of the predicted parameters in Table II. To have a graphical understanding of the predicted parameters, we highlight the plots for the same in Fig. 2. In Fig. 3, we highlight the plots of $Re[s], Im[s], Re[t]$. So far,

| Prediction | δ | m_1 | m_2 | m_3 | $\sum m_i$ | α | β | J_{CP} |
|------------|---------------|----------|----------|----------|------------|-------------|---------------|-----------|
| Minimum | 285.7° | 0.021 eV | 0.023 eV | 0.053 eV | 0.1 eV | -90° | -12.7° | -0.0324 |
| Maximum | 421° | 0.030 eV | 0.031 eV | 0.058 eV | 0.118 eV | 90° | 13.6° | 0.030 |

TABLE II. The approximate minimum and maximum values of $\delta, m_1, m_2, m_3, \sum m_i, \alpha, \beta$, and J_{CP} as predicted by the model.

we have presented the predictions for the low energy observable quantities as well as the texture parameters $Re[s], Im[s]$, and $Re[t]$. These texture parameters, however, are not arbitrary, they are generated from a deeper set of model parameters, including the Yukawa couplings and flavon vevs, as outlined in Eqs. (8)–(12). Therefore, by using the predicted values of the texture parameters, we can determine or constrain the underlying model parameters that define the theory at a more fundamental level. Though the framework cannot directly predict the individual model parameters, it can provide numerical information for several interesting combinations of them. In this connection, we highlight the model parameter combinations below, which are functions of the free parameters $Re[s], Im[s]$, and $Re[t]$

$$\begin{aligned} G_1 &= \frac{y_{D_1} v_\Phi}{\sqrt{M_1}}, & G_2 &= \frac{y_{D_2} v_\Phi v_\sigma}{\sqrt{y_2 v_\kappa \Lambda}}, & G_3 &= \frac{y_{D_3} v_\Phi v_\rho}{\sqrt{y_3 v_\chi \Lambda}}, \\ G_4 &= \frac{y_1 v_\zeta}{\sqrt{y_2 y_3 v_\kappa v_\chi}}, & G_5 &= y_\Delta v_\Delta. \end{aligned} \quad (19)$$

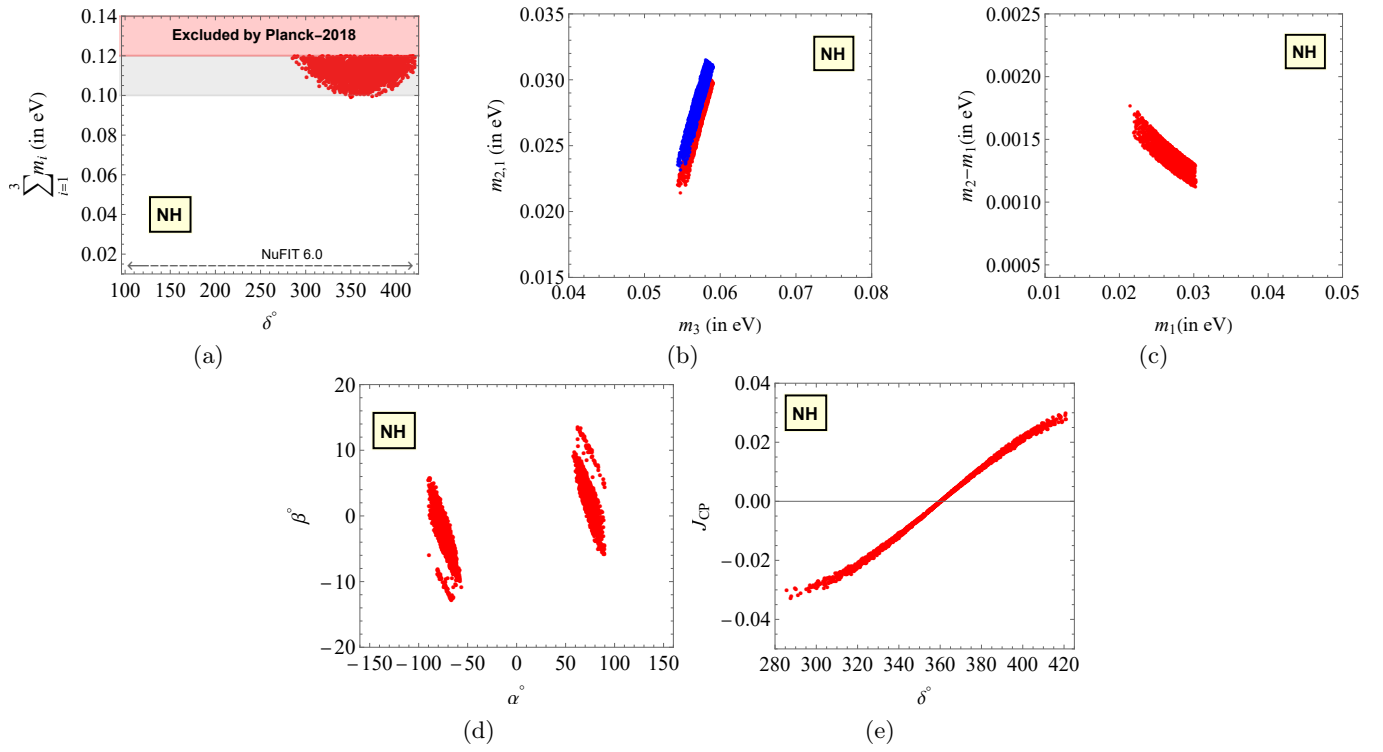


FIG. 2. The plots of the predicted parameters are shown. (a) δ vs $\sum m_i$. (b) $m_{2,1}$ vs m_3 . (c) $m_2 - m_1$ vs m_1 . (d) α vs β . (e) δ vs J_{CP} .

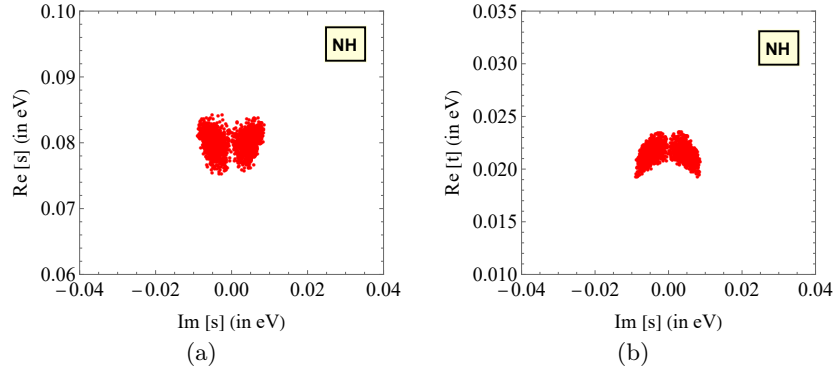


FIG. 3. The plots of the free parameters are shown. (a) $Im[s]$ vs $Re[s]$. (b) $Im[s]$ vs $Re[t]$.

| Parameter | $ G_1 $ | $ G_2 $ | $ G_3 $ | $ G_4 $ | $ G_5 $ | $Arg[G_1]$ | $Arg[G_2]$ | $Arg[G_3]$ | $Arg[G_4]$ | $Arg[G_5]$ |
|-----------|----------------------------------|----------------------------------|----------------------------------|---------|-----------|-----------------|-----------------|-----------------|-----------------|-----------------|
| Minimum | $0.156 \text{ eV}^{\frac{1}{2}}$ | $0.05 \text{ eV}^{\frac{1}{2}}$ | $0.025 \text{ eV}^{\frac{1}{2}}$ | 0.118 | 0.060 eV | -90.000° | -92.364° | -92.854° | -42.100° | -21.170° |
| Maximum | $0.253 \text{ eV}^{\frac{1}{2}}$ | $0.355 \text{ eV}^{\frac{1}{2}}$ | $0.224 \text{ eV}^{\frac{1}{2}}$ | 1.185 | 0.0722 eV | 90.000° | 92.233° | 92.767° | 50.000° | 23.000° |

TABLE III. The approximate maximum and minimum values of the model parameter combinations.

The predicted numerical values of the model parameter combinations G_1, G_2, G_3, G_4 , and G_5 are listed in Table III. To visualise these combinations graphically, we plot them in Fig. 4.

The model is now equipped with all the necessary numerical inputs to examine its consistency in light of low energy phenomenologies such as $0\nu\beta\beta$ decay and cLFV.

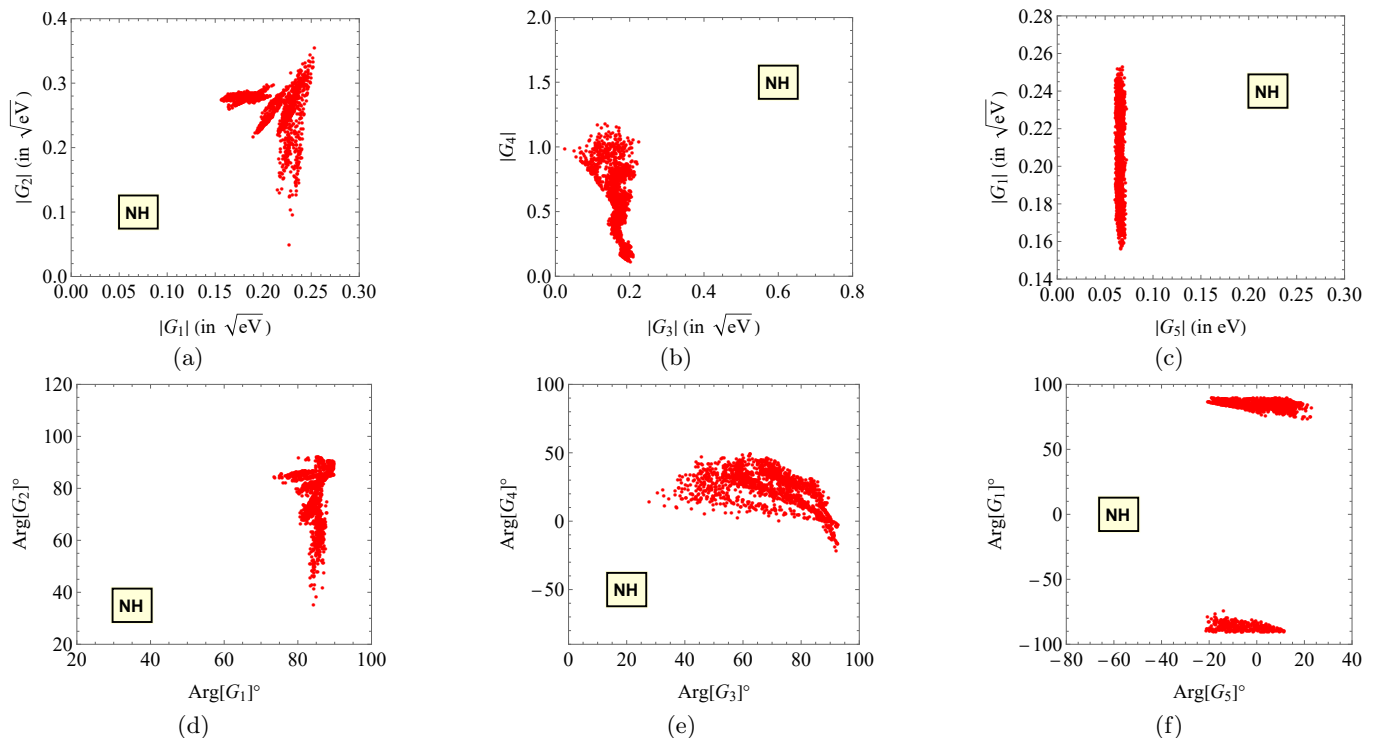


FIG. 4. The plots of the model parameter combinations are shown.

IV. NEUTRINOLESS DOUBLE BETA DECAY

The model adheres to the Majorana nature of the neutrinos, therefore, it is pertinent to discuss the effective Majorana mass, $m_{\beta\beta}$. This quantity is a crucial observable in determining the half life ($T_{1/2}$) of $0\nu\beta\beta$ decay [41–43]. The $0\nu\beta\beta$ decay is a hypothetical decay in which an unstable nucleus undergoes two simultaneous beta decays without emitting neutrinos. Such a decay is only possible if neutrinos are Majorana particles. A typical Feynman diagram for this process is shown in Fig. 5. A confirmed observation of this process would thus provide direct evidence for the Majorana nature of neutrinos. Although no positive signal has been observed to date, several experiments have placed stringent upper limits on the observable $m_{\beta\beta}$, which are summarised in Table IV. The general expression for $m_{\beta\beta}$ is given below

$$m_{\beta\beta} = |U_{ei}^2 m_i|, \quad \text{where, } i = 1, 2, 3. \quad (20)$$

As mentioned previously, $Re[s]$, $Im[s]$, and $Re[t]$ dictate the structure of M_ν and all associated predictions. Hence,

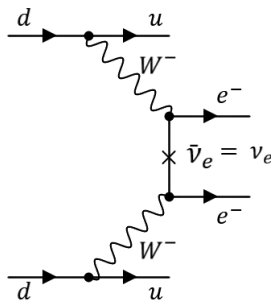


FIG. 5. Feynman diagram for $0\nu\beta\beta$ decay.

$m_{\beta\beta}$ is no exception. For NH, the model places stringent bound on $m_{\beta\beta}$, predicting it to lie within the range 0.0060 eV – 0.0227 eV. This range is consistent with the current upper limits set by KamLAND-Zen and GERDA, and lies

| Isotope | ^{130}Te | ^{136}Xe | ^{76}Ge | ^{136}Xe | ^{76}Ge |
|-----------------------|-------------------|-------------------|------------------|------------------------------|------------------|
| $m_{\beta\beta}$ (eV) | < 0.09–0.305 | < 0.093–0.286 | < 0.08–0.18 | < 0.061–0.165, < 0.036–0.156 | < 0.009–0.021 |
| Collaboration | CUORE [44] | EXO [45] | GERDA [46] | KamLAND-Zen [47, 48] | LEGEND-1000 [49] |

TABLE IV. The present upper limits on $m_{\beta\beta}$ from $0\nu\beta\beta$ decay searches in different isotopes.

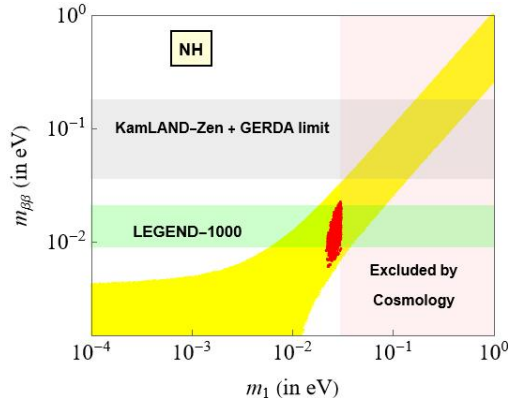


FIG. 6. The plot of $m_{\beta\beta}$ versus m_1 . In the plot, the ‘yellow’ area show the generic region allowed by current oscillation data in case of NH. The ‘gray’ band indicates the bounds on $m_{\beta\beta}$ set by KamLAND-Zen and GERDA. The ‘faded pink’ band corresponds to the region excluded by cosmology in case of NH. The ‘light green’ band shows the projected sensitivity of the LEGEND-1000, and the ‘red’ curve represents the prediction of the present model.

within the projected sensitivity of the LEGEND-1000 experiment. To visualise the prediction of $m_{\beta\beta}$ by the model, we show the plot of $m_{\beta\beta}$ versus the lightest neutrino mass eigenvalue (m_1) in Fig. 6

V. CHARGED LEPTON FLAVOUR VIOLATION

In the SM of particle physics, cLFV processes [50–63] are highly suppressed, with predicted branching ratios around 10^{-50} . Therefore, cLFV is one of the most promising probes of physics beyond the SM. Among the various decay channels, transitions involving muons are the most interesting, as muons have a longer lifetime than other leptons and are abundantly produced in cosmic radiation. This makes muon decays ideal for study. So far, there is no experimental evidence of cLFV decays. However, ongoing experiments are steadily improving their sensitivities to search for these rare processes. To complement these experimental efforts, it is worthwhile to explore theoretical frameworks that could explain or predict such decays. As an extension of our model, we plan to study the dominant decay $\mu \rightarrow e\gamma$. The current best limit on the branching ratio of the $\mu \rightarrow e\gamma$ decay is provided by MEG [64]

$$\text{BR}(\mu \rightarrow e\gamma) < 4.2 \times 10^{-13}. \quad (21)$$

The MEG II [65–67] experiment is currently searching for this rare decay at the Paul Scherrer Institute (PSI) muon beam facility. Its goal is to improve the sensitivity of measurements to $\text{BR}(\mu \rightarrow e\gamma) \sim 6 \times 10^{-14}$ by the end of 2026. In the present model, it is possible to explore how each seesaw mechanism may contribute to the $\mu \rightarrow e\gamma$ decay. We then aim to determine which contribution is the dominant one. In the case of Type-I seesaw, the $\mu \rightarrow e\gamma$ decay arises due to the existence of heavy-light neutrino mixing. To understand this, we write the effective Lagrangian for the Type-I seesaw in the following manner

$$\mathcal{L}_\nu = \frac{1}{2} \bar{n}^c M n + h.c., \quad (22)$$

with

$$n = \begin{pmatrix} \nu_L^c \\ \nu_R \end{pmatrix}, \quad (23)$$

and the 6×6 mass matrix,

$$M = \begin{pmatrix} 0 & M_D \\ M_D^T & M_R \end{pmatrix}. \quad (24)$$

The block diagonalisation of M is achieved by the following transformation

$$\begin{pmatrix} 1 - \frac{RR^\dagger}{2} & R \\ -R^\dagger & 1 - \frac{RR^\dagger}{2} \end{pmatrix}^T \begin{pmatrix} 0 & M_D \\ M_D^T & M_R \end{pmatrix} \begin{pmatrix} 1 - \frac{RR^\dagger}{2} & R \\ -R^\dagger & 1 - \frac{RR^\dagger}{2} \end{pmatrix} \simeq \begin{pmatrix} m_{\text{light}} & 0 \\ 0 & M_{\text{heavy}} \end{pmatrix}, \quad (25)$$

where $R = M_D^\dagger M_R^{-1}$, $m_{\text{light}} = -M_D M_R^{-1} M_D^T$ and $M_{\text{heavy}} = M_R$. The next step is to diagonalise the block diagonalised matrix in Eq. 25. This is achieved via the transformation below

$$\begin{pmatrix} U & 0 \\ 0 & U_R \end{pmatrix}^T \begin{pmatrix} m_{\text{light}} & 0 \\ 0 & M_{\text{heavy}} \end{pmatrix} \begin{pmatrix} U & 0 \\ 0 & U_R \end{pmatrix} \simeq \begin{pmatrix} \text{diag}(m_i) & 0 \\ 0 & \text{diag}(M_i) \end{pmatrix}, \quad (26)$$

where U is the PMNS matrix that diagonalises m_{light} , and U_R diagonalises M_{heavy} . This two step diagonalisation of M can be simplified to a single step in the following way

$$\begin{pmatrix} U & 0 \\ 0 & U_R \end{pmatrix}^T \begin{pmatrix} 1 - \frac{RR^\dagger}{2} & R \\ -R^\dagger & 1 - \frac{RR^\dagger}{2} \end{pmatrix}^T \begin{pmatrix} 0 & M_D \\ M_D^T & M_R \end{pmatrix} \begin{pmatrix} 1 - \frac{RR^\dagger}{2} & R \\ -R^\dagger & 1 - \frac{RR^\dagger}{2} \end{pmatrix} \begin{pmatrix} U & 0 \\ 0 & U_R \end{pmatrix} \simeq \begin{pmatrix} \text{diag}(m_i) & 0 \\ 0 & \text{diag}(M_i) \end{pmatrix}. \quad (27)$$

Therefore, M can be diagonalised by the matrix

$$D = \begin{pmatrix} (1 - \frac{RR^\dagger}{2})U & RU_R \\ -R^\dagger U & (1 - \frac{RR^\dagger}{2})U_R \end{pmatrix}, \quad (28)$$

and the off diagonal part $K = RU_R = M_D^\dagger M_R^{-1} U_R$ carries the information of heavy-light neutrino mixing. In the case of the Type-I seesaw, K directly enters the expression for the branching ratio of the $\mu \rightarrow e\gamma$ decay, which is given by [68–73]

$$BR(\mu \rightarrow e\gamma) = \frac{3\alpha_f}{8\pi} \left| \sum_i K_{ei} K_{i\mu}^\dagger F\left(\frac{M_i^2}{M_W^2}\right) \right|^2, \quad (29)$$

where, α_f stands for the fine structure constant, M_i is the mass of the i^{th} right handed neutrino, and M_W is the mass of W boson. The factor $F(x)$ is expressed as

$$F(x) = \frac{x(1 - 6x + 3x^2 + 2x^3 - 6x^2 \ln x)}{2(1 - x)^4}, \quad (30)$$

where, $x = \frac{M_i^2}{M_W^2}$. To compute $BR(\mu \rightarrow e\gamma)$, we consider M_R in the TeV range, requiring $M_D \sim \text{MeV}$ to reproduce light neutrino masses $\sim 10^{-2}$ eV. This leads to $BR(\mu \rightarrow e\gamma) \sim \mathcal{O}(10^{-40})$, far below the experimental limit. Hence, the Type-I contribution to $BR(\mu \rightarrow e\gamma)$ is insignificant.

With this inference in mind, we now turn our attention to the Type-II seesaw contribution to $BR(\mu \rightarrow e\gamma)$. In this case, the process arises at the one loop level, mediated by the singly and doubly charged components of the scalar triplet Δ . The corresponding branching ratio is given by [63, 74, 75]

$$BR(\mu \rightarrow e\gamma) = \frac{\alpha_f |(Y_{II}^* Y_{II})_{e\mu}|^2}{192\pi G_F^2} \left(\frac{1}{m_{\Delta^\pm}^2} + \frac{8}{m_{\Delta^{\pm\pm}}^2} \right)^2, \quad (31)$$

where Y_{II} is the Type-II Yukawa matrix, and G_F denotes the Fermi constant. In our analysis, we assume that the charged components of the scalar triplet are approximately degenerate in mass, i.e., $m_{\Delta^{++}} \simeq m_{\Delta^+} \simeq m_{\Delta}$. This assumption is well justified in scenarios where the mass splitting among triplet components is small. Substituting the model predicted value of $(Y_{II}^* Y_{II})_{e\mu}$ into Eq. (31), the branching ratio simplifies to

$$BR(\mu \rightarrow e\gamma) \simeq 0.0208 \frac{\alpha_f}{\pi G_F^2} \left(\frac{|G_5|}{m_{\Delta} v_{\Delta}} \right)^4. \quad (32)$$

From Eq. (32), it is evident that the branching ratio depends on the parameters $|G_5|$, m_Δ , and v_Δ . Using the numerical values of $|G_5|$ obtained from our model, we perform a scan over m_Δ and v_Δ to identify the regions of parameter space that yield branching ratios consistent with experimental limits. This allows us to determine the most favourable regions in the $(m_\Delta, v_\Delta, |G_5|)$ parameter space. Based on our numerical analysis, we find that the predicted branching ratio $BR(\mu \rightarrow e\gamma)$ lies within the range $[10^{-15}, 4 \times 10^{-13}]$, which is compatible with the current MEG bound and the projected sensitivity of MEG-II. While $|G_5|$ remains fixed within its allowed range $[0.06, 0.072]$ eV, three distinct and viable sets of bounds for m_Δ and v_Δ emerge, as summarised in Table V. The HL-LHC [76], HE-LHC [77] and

| | | $ G_5 \in [0.06, 0.072]$ eV | | |
|-----|----------|---|---------|------------|
| | | $BR(\mu \rightarrow e\gamma) \in [10^{-15}, 4 \times 10^{-13}]$ | | |
| | | m_Δ | | v_Δ |
| Set | Minimum | Maximum | Minimum | Maximum |
| A | 870 GeV | 4 TeV | 2.30 eV | 2.50 eV |
| B | 1.00 TeV | 4.50 TeV | 1.98 eV | 2.10 eV |
| C | 1.20 TeV | 8.70 TeV | 1.00 eV | 1.70 eV |

TABLE V. Numerical sets of (m_Δ, v_Δ) yielding $BR(\mu \rightarrow e\gamma) \in [10^{-15}, 4 \times 10^{-13}]$ for $|G_5| \in [0.06, 0.072]$ eV.

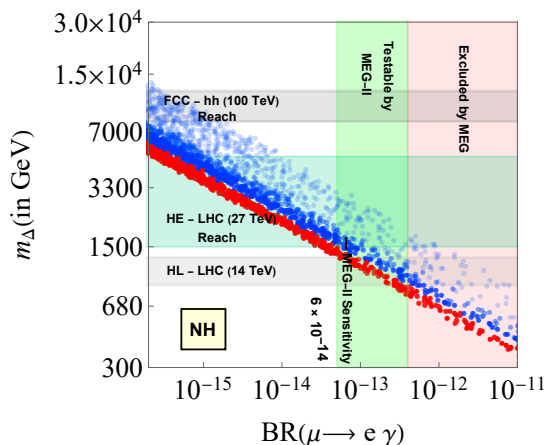


FIG. 7. The plot of $BR(\mu \rightarrow e\gamma)$ vs. m_Δ . The ‘red’, ‘blue’, and ‘faded blue’ points represent the predicted ranges of $BR(\mu \rightarrow e\gamma)$ for set A, set B, and set C, respectively. The ‘faded red’ region is excluded by the MEG experiment, while the ‘pale green’ region indicates the $BR(\mu \rightarrow e\gamma)$ values that are within reach of MEG-II sensitivity. The potential reach of high-energy colliders such as HL-LHC, HE-LHC, and FCC-hh is also overlaid for comparison.

FCC-hh [78] are expected to probe the higher mass range of the scalar triplet Δ . In particular, the collider signatures of $\Delta^{\pm\pm}$ [79], such as same-sign dilepton decays ($\Delta^{\pm\pm} \rightarrow \ell^\pm \ell^\pm$) for small v_Δ , and diboson decays ($\Delta^{\pm\pm} \rightarrow W^\pm W^\pm$) for larger v_Δ , provide promising avenues to test the scalar triplet mass. These searches, combined with charged lepton flavour violation, can play a crucial role in probing the parameter space of our model. To visualize our findings, we present a plot of $BR(\mu \rightarrow e\gamma)$ as a function of m_Δ in Fig. 7. Therefore, we may infer that in our model the dominant contribution to the $BR(\mu \rightarrow e\gamma)$ comes from the Type-II seesaw mechanism.

VI. SUMMARY AND DISCUSSIONS

We have presented a flavour driven neutrino mass model that stands out by generating a distinctive and predictive *Echo 12-23 Texture*, realized from first principles within a Type-I+II seesaw framework. This elegant texture emerges naturally from an extended symmetry structure, $A_4 \times Z_3 \times Z_{10}$, which plays a crucial role in shaping the Yukawa sector and suppressing unwanted contributions via higher dimensional operators. Remarkably, the model accounts for the lepton mass hierarchy and predicts the entire neutrino mass matrix using just three real input parameters. The model makes sharp predictions for the three neutrino mass eigenvalues, as well as the Dirac and Majorana CP phases.

Furthermore, it yields consistent predictions for the effective neutrino mass in light of $0\nu\beta\beta$ decay and the branching ratio of the dominant $\mu \rightarrow e\gamma$ decay. This opens up prospects for verification in current and upcoming experiments. Overall, this framework offers a fresh path toward decoding the flavour puzzle in the lepton sector.

ACKNOWLEDGEMENT

The research work of MD is financially supported by Council of Scientific and Industrial Research (CSIR), Government of India through a NET Senior Research Fellowship vide grant No. 09/0059(15346)/2022-EMR-I.

-
- [1] S. L. Glashow, Partial Symmetries of Weak Interactions, Nucl. Phys. **22**, 579 (1961).
 - [2] S. Weinberg, A Model of Leptons, Phys. Rev. Lett. **19**, 1264 (1967).
 - [3] A. Salam, Weak and Electromagnetic Interactions, Conf. Proc. C **680519**, 367 (1968).
 - [4] D. J. Gross and F. Wilczek, Ultraviolet Behavior of Nonabelian Gauge Theories, Phys. Rev. Lett. **30**, 1343 (1973).
 - [5] H. D. Politzer, Reliable Perturbative Results for Strong Interactions?, Phys. Rev. Lett. **30**, 1346 (1973).
 - [6] C. L. Cowan, F. Reines, F. B. Harrison, H. W. Kruse, and A. D. McGuire, Detection of the free neutrino: A Confirmation, Science **124**, 103 (1956).
 - [7] Q. R. Ahmad *et al.* (SNO), Direct evidence for neutrino flavor transformation from neutral current interactions in the Sudbury Neutrino Observatory, Phys. Rev. Lett. **89**, 011301 (2002), arXiv:nucl-ex/0204008.
 - [8] K. Eguchi *et al.* (KamLAND), First results from KamLAND: Evidence for reactor anti-neutrino disappearance, Phys. Rev. Lett. **90**, 021802 (2003), arXiv:hep-ex/0212021.
 - [9] Y. Fukuda *et al.* (Super-Kamiokande), Measurement of the flux and zenith angle distribution of upward through going muons by Super-Kamiokande, Phys. Rev. Lett. **82**, 2644 (1999), arXiv:hep-ex/9812014.
 - [10] M. Yoshimura, Unified Gauge Theories and the Baryon Number of the Universe, Phys. Rev. Lett. **41**, 281 (1978), [Erratum: Phys.Rev.Lett. **42**, 746 (1979)].
 - [11] E. K. Akhmedov, G. C. Branco, and M. N. Rebelo, Seesaw mechanism and structure of neutrino mass matrix, Phys. Lett. B **478**, 215 (2000), arXiv:hep-ph/9911364.
 - [12] R. N. Mohapatra, Seesaw mechanism and its implications, in *SEESAW25: International Conference on the Seesaw Mechanism and the Neutrino Mass* (2004) pp. 29–44, arXiv:hep-ph/0412379.
 - [13] S. F. King, Neutrino mass models, Rept. Prog. Phys. **67**, 107 (2004), arXiv:hep-ph/0310204.
 - [14] T. P. Cheng and L.-F. Li, Neutrino Masses, Mixings and Oscillations in SU(2) x U(1) Models of Electroweak Interactions, Phys. Rev. D **22**, 2860 (1980).
 - [15] Y. Cai, T. Han, T. Li, and R. Ruiz, Lepton Number Violation: Seesaw Models and Their Collider Tests, Front. in Phys. **6**, 40 (2018), arXiv:1711.02180 [hep-ph].
 - [16] E. K. Akhmedov and M. Frigerio, Interplay of type I and type II seesaw contributions to neutrino mass, JHEP **01**, 043, arXiv:hep-ph/0609046.
 - [17] S. Verma, M. Kashav, and S. Bhardwaj, Highly predictive and testable A_4 flavor model within type-I and II seesaw framework and associated phenomenology, Nucl. Phys. B **946**, 114704 (2019), arXiv:1811.06249 [hep-ph].
 - [18] L. Singh, Tapender, M. Kashav, and S. Verma, Trimaximal mixing and extended magic symmetry in a model of neutrino mass matrix, EPL **142**, 64002 (2023), arXiv:2207.13328 [hep-ph].
 - [19] P. Ramond, R. G. Roberts, and G. G. Ross, Stitching the Yukawa quilt, Nucl. Phys. B **406**, 19 (1993), arXiv:hep-ph/9303320.
 - [20] H. Fritzsch, Z.-z. Xing, and S. Zhou, Two-zero Textures of the Majorana Neutrino Mass Matrix and Current Experimental Tests, JHEP **09**, 083, arXiv:1108.4534 [hep-ph].
 - [21] P. O. Ludl and W. Grimus, A complete survey of texture zeros in the lepton mass matrices, JHEP **07**, 090, [Erratum: JHEP **10**, 126 (2014)], arXiv:1406.3546 [hep-ph].
 - [22] P. F. Harrison, D. H. Perkins, and W. G. Scott, Tri-bimaximal mixing and the neutrino oscillation data, Phys. Lett. B **530**, 167 (2002), arXiv:hep-ph/0202074.
 - [23] Z.-z. Xing, The μ - τ reflection symmetry of Majorana neutrinos *, Rept. Prog. Phys. **86**, 076201 (2023), arXiv:2210.11922 [hep-ph].
 - [24] E. Ma and G. Rajasekaran, Softly broken A(4) symmetry for nearly degenerate neutrino masses, Phys. Rev. D **64**, 113012 (2001), arXiv:hep-ph/0106291.
 - [25] S. F. King and M. Malinsky, A(4) family symmetry and quark-lepton unification, Phys. Lett. B **645**, 351 (2007), arXiv:hep-ph/0610250.
 - [26] G. Altarelli and F. Feruglio, Discrete Flavor Symmetries and Models of Neutrino Mixing, Rev. Mod. Phys. **82**, 2701 (2010), arXiv:1002.0211 [hep-ph].
 - [27] S. F. King and C. Luhn, Neutrino Mass and Mixing with Discrete Symmetry, Rept. Prog. Phys. **76**, 056201 (2013), arXiv:1301.1340 [hep-ph].
 - [28] E. Ma, Lepton family symmetry and neutrino mass matrix, Mod. Phys. Lett. A **19**, 577 (2004), arXiv:hep-ph/0401025.

- [29] B. Hu, F. Wu, and Y.-L. Wu, $Z(3)$ Symmetry and Neutrino Mixing in Type II Seesaw, *Phys. Rev. D* **75**, 113003 (2007), arXiv:hep-ph/0612344.
- [30] A. E. Cárcamo Hernández and I. de Medeiros Varzielas, $\Delta(27)$ framework for cobimaximal neutrino mixing models, *Phys. Lett. B* **806**, 135491 (2020), arXiv:2003.01134 [hep-ph].
- [31] M. Dey and S. Roy, A realistic neutrino mixing scheme arising from A_4 symmetry, *EPL* **147**, 14002 (2024), arXiv:2304.07259 [hep-ph].
- [32] M. Dey and S. Roy, Revisiting the Dirac nature of neutrinos in the light of $\Delta(27)$ and cyclic symmetries, *J. Phys. G* **52**, 025005 (2025), arXiv:2403.12461 [hep-ph].
- [33] V. V. Van, $A_4 \times Z_2 \times Z_4$ flavor symmetry model for neutrino oscillation phenomenology, *Rev. Mex. Fis.* **70**, 060801 (2024).
- [34] C. D. Froggatt and H. B. Nielsen, Hierarchy of Quark Masses, Cabibbo Angles and CP Violation, *Nucl. Phys. B* **147**, 277 (1979).
- [35] K. S. Babu and S. Nandi, Natural fermion mass hierarchy and new signals for the Higgs boson, *Phys. Rev. D* **62**, 033002 (2000), arXiv:hep-ph/9907213.
- [36] M. Tanabashi *et al.* (Particle Data Group), Review of Particle Physics, *Phys. Rev. D* **98**, 030001 (2018).
- [37] R. L. Workman *et al.* (Particle Data Group), Review of Particle Physics, *PTEP* **2022**, 083C01 (2022).
- [38] Z. Maki, M. Nakagawa, and S. Sakata, Remarks on the unified model of elementary particles, *Prog. Theor. Phys.* **28**, 870 (1962).
- [39] I. Esteban, M. C. Gonzalez-Garcia, M. Maltoni, I. Martinez-Soler, J. a. P. Pinheiro, and T. Schwetz, NuFit-6.0: updated global analysis of three-flavor neutrino oscillations, *JHEP* **12**, 216, arXiv:2410.05380 [hep-ph].
- [40] N. Aghanim *et al.* (Planck), Planck 2018 results. VI. Cosmological parameters, *Astron. Astrophys.* **641**, A6 (2020), [Erratum: *Astron. Astrophys.* 652, C4 (2021)], arXiv:1807.06209 [astro-ph.CO].
- [41] J. Schechter and J. W. F. Valle, Neutrinoless Double beta Decay in $SU(2) \times U(1)$ Theories, *Phys. Rev. D* **25**, 2951 (1982).
- [42] M. Blennow, E. Fernandez-Martinez, J. Lopez-Pavon, and J. Menendez, Neutrinoless double beta decay in seesaw models, *JHEP* **07**, 096, arXiv:1005.3240 [hep-ph].
- [43] A. Barabash, Double Beta Decay Experiments: Recent Achievements and Future Prospects, *Universe* **9**, 290 (2023).
- [44] D. Q. Adams *et al.* (CUORE), Search for Majorana neutrinos exploiting millikelvin cryogenics with CUORE, *Nature* **604**, 53 (2022), arXiv:2104.06906 [nucl-ex].
- [45] G. Anton *et al.* (EXO-200), Search for Neutrinoless Double- β Decay with the Complete EXO-200 Dataset, *Phys. Rev. Lett.* **123**, 161802 (2019), arXiv:1906.02723 [hep-ex].
- [46] M. Agostini *et al.* (GERDA), Final Results of GERDA on the Search for Neutrinoless Double- β Decay, *Phys. Rev. Lett.* **125**, 252502 (2020), arXiv:2009.06079 [nucl-ex].
- [47] A. Gando *et al.* (KamLAND-Zen), Search for Majorana Neutrinos near the Inverted Mass Hierarchy Region with KamLAND-Zen, *Phys. Rev. Lett.* **117**, 082503 (2016), [Addendum: *Phys. Rev. Lett.* 117, 109903 (2016)], arXiv:1605.02889 [hep-ex].
- [48] S. Abe *et al.* (KamLAND-Zen), Search for the Majorana Nature of Neutrinos in the Inverted Mass Ordering Region with KamLAND-Zen, *Phys. Rev. Lett.* **130**, 051801 (2023), arXiv:2203.02139 [hep-ex].
- [49] N. Abgrall *et al.* (LEGEND), The Large Enriched Germanium Experiment for Neutrinoless $\beta\beta$ Decay: LEGEND-1000 Preconceptual Design Report, (2021), arXiv:2107.11462 [physics.ins-det].
- [50] L. Calibbi and G. Signorelli, Charged Lepton Flavour Violation: An Experimental and Theoretical Introduction, *Riv. Nuovo Cim.* **41**, 71 (2018), arXiv:1709.00294 [hep-ph].
- [51] M. Ardu and G. Pezzullo, Introduction to Charged Lepton Flavor Violation, *Universe* **8**, 299 (2022), arXiv:2204.08220 [hep-ph].
- [52] F. Ci and D. Nicolo, Lepton Flavour Violation Experiments, *Adv. High Energy Phys.* **2014**, 282915 (2014).
- [53] A. Matsuzaki and H. Tanaka, Lepton Flavor Violating $\tau \rightarrow 3\mu$ Decay in Type-III Two Higgs Doublet Model, *Phys. Rev. D* **79**, 015006 (2009), arXiv:0809.3072 [hep-ph].
- [54] A. G. Akeroyd, M. Aoki, and H. Sugiyama, Lepton Flavour Violating Decays $\tau \rightarrow \text{anti-l ll}$ and $\mu \rightarrow e \gamma$ in the Higgs Triplet Model, *Phys. Rev. D* **79**, 113010 (2009), arXiv:0904.3640 [hep-ph].
- [55] A. Celis, V. Cirigliano, and E. Passemar, Lepton flavor violation in the higgs sector and the role of hadronic τ -lepton decays, *Phys. Rev. D* **89**, 013008 (2014).
- [56] L. T. Hue, D. T. Huong, and H. N. Long, Lepton flavor violating processes $\tau \rightarrow \mu\gamma$, $\tau \rightarrow 3\mu$ and $Z \rightarrow \mu\tau$ in the Supersymmetric economical 3-3-1 model, *Nucl. Phys. B* **873**, 207 (2013), arXiv:1301.4652 [hep-ph].
- [57] D. N. Dinh and S. T. Petcov, Lepton Flavor Violating τ Decays in TeV Scale Type I See-Saw and Higgs Triplet Models, *JHEP* **09**, 086, arXiv:1308.4311 [hep-ph].
- [58] Y. Omura, E. Senaha, and K. Tobe, τ - and μ -physics in a general two Higgs doublet model with $\mu - \tau$ flavor violation, *Phys. Rev. D* **94**, 055019 (2016), arXiv:1511.08880 [hep-ph].
- [59] H. Zhou, R.-Y. Zhang, L. Han, W.-G. Ma, L. Guo, and C. Chen, Searching for $\tau \rightarrow \mu\gamma$ lepton-flavor-violating decay at super charm-tau factory, *Eur. Phys. J. C* **76**, 421 (2016), arXiv:1602.01181 [hep-ph].
- [60] C. O. Dib, T. Gutsche, S. G. Kovalenko, V. E. Lyubovitskij, and I. Schmidt, Bounds on lepton flavor violating physics and decays of neutral mesons from $\tau(\mu) \rightarrow 3\ell$, $\ell\gamma\gamma$ -decays, *Phys. Rev. D* **99**, 035020 (2019).
- [61] G. Hernández-Tomé, G. López Castro, and P. Roig, Flavor violating leptonic decays of τ and μ leptons in the Standard Model with massive neutrinos, *Eur. Phys. J. C* **79**, 84 (2019), [Erratum: *Eur. Phys. J. C* 80, 438 (2020)], arXiv:1807.06050 [hep-ph].
- [62] Z. Calcuttawala, A. Kundu, S. Nandi, and S. Kumar Patra, New physics with the lepton flavor violating decay $\tau \rightarrow 3\mu$, *Phys. Rev. D* **97**, 095009 (2018), arXiv:1802.09218 [hep-ph].

- [63] M. M. Ferreira, T. B. de Melo, S. Kovalenko, P. R. D. Pinheiro, and F. S. Queiroz, Lepton Flavor Violation and Collider Searches in a Type I + II Seesaw Model, *Eur. Phys. J. C* **79**, 955 (2019), arXiv:1903.07634 [hep-ph].
- [64] A. M. Baldini *et al.* (MEG), Search for the lepton flavour violating decay $\mu^+ \rightarrow e + \gamma$ with the full dataset of the MEG experiment, *Eur. Phys. J. C* **76**, 434 (2016), arXiv:1605.05081 [hep-ex].
- [65] M. Meucci (MEG II), MEG II experiment status and prospect, PoS **NuFact2021**, 120 (2022), arXiv:2201.08200 [hep-ex].
- [66] K. Afanaciev *et al.* (MEG II), A search for $\mu^+ \rightarrow e + \gamma$ with the first dataset of the MEG II experiment, *Eur. Phys. J. C* **84**, 216 (2024), arXiv:2310.12614 [hep-ex].
- [67] M. Francesconi (MEG II), Status of the MEG II experiment, PoS **EPS-HEP2023**, 355 (2024).
- [68] S. M. Bilenky, S. T. Petcov, and B. Pontecorvo, Lepton Mixing, $\mu \rightarrow e + \gamma$ Decay and Neutrino Oscillations, *Phys. Lett. B* **67**, 309 (1977).
- [69] A. Ilakovac and A. Pilaftsis, Flavor violating charged lepton decays in seesaw-type models, *Nucl. Phys. B* **437**, 491 (1995), arXiv:hep-ph/9403398.
- [70] D. Tommasini, G. Barenboim, J. Bernabeu, and C. Jarlskog, Nondecoupling of heavy neutrinos and lepton flavor violation, *Nucl. Phys. B* **444**, 451 (1995), arXiv:hep-ph/9503228.
- [71] D. V. Forero, S. Morisi, M. Tortola, and J. W. F. Valle, Lepton flavor violation and non-unitary lepton mixing in low-scale type-I seesaw, *JHEP* **09**, 142, arXiv:1107.6009 [hep-ph].
- [72] A. Datta, B. Karmakar, and A. Sil, Flavored leptogenesis and neutrino mass with A_4 symmetry, *JHEP* **12**, 051, arXiv:2106.06773 [hep-ph].
- [73] M. Dey and S. Roy, Unveiling neutrino mysteries with $\Delta(27)$ symmetry, *Phys. Lett. B* **864**, 139401 (2025), arXiv:2309.14769 [hep-ph].
- [74] D. N. Dinh, A. Ibarra, E. Molinaro, and S. T. Petcov, The $\mu - e$ Conversion in Nuclei, $\mu \rightarrow e\gamma$, $\mu \rightarrow 3e$ Decays and TeV Scale See-Saw Scenarios of Neutrino Mass Generation, *JHEP* **08**, 125, [Erratum: *JHEP* 09, 023 (2013)], arXiv:1205.4671 [hep-ph].
- [75] N. D. Barrie and S. T. Petcov, Lepton Flavour Violation tests of Type II Seesaw Leptogenesis, *JHEP* **01**, 001, arXiv:2210.02110 [hep-ph].
- [76] High-Luminosity Large Hadron Collider (HL-LHC) : Preliminary Design Report 10.5170/CERN-2015-005 (2015).
- [77] M. Benedikt and F. Zimmermann, Proton Colliders at the Energy Frontier, *Nucl. Instrum. Meth. A* **907**, 200 (2018), arXiv:1803.09723 [physics.acc-ph].
- [78] A. Abada *et al.* (FCC), FCC-hh: The Hadron Collider: Future Circular Collider Conceptual Design Report Volume 3, *Eur. Phys. J. ST* **228**, 755 (2019).
- [79] S. Antusch, O. Fischer, A. Hammad, and C. Scherb, Low scale type II seesaw: Present constraints and prospects for displaced vertex searches, *JHEP* **02**, 157, arXiv:1811.03476 [hep-ph].